METALS AND MATERIALS International, Vol. 10, No. 1 (2004), pp. 1~5

Amorphous Phase Formation in a Ni-Zr-Al-Y Alloy System

W. B. Kim, B. J. Ye, and S. Yi*

Department of Materials Science and Metallurgy, Kyungpook National University
1370 Sangyeok 3-dong, Buk-gu, Daegu 702-701, Korea

Quaternary Ni-based amorphous alloys containing only metallic elements were developed through systematic alloy design. The importance of the phase equilibria information for the development of amorphous alloys was demonstrated through experimental results. Ni-Zr-Al ternary alloys having low liquidus temperature tend to have high GFA. Partial replacements of Zr with Y in the ternary alloys significantly enhanced the GFA of the quaternary alloys. The alloy $Ni_{60}Zr_{25}Al_8Y_7$ could be cast into a fully amorphous rod through an injection casting method. Since most Ni-based amorphous alloys reported to date contain non-metallic elements, the Ni-based amorphous alloys developed in the alloy system Ni-Zr-Al-Y are of interest.

Keywords: Ni-based amorphous, phase equilibria, GFA (Glass Forming Ability), Ni-Zr-Al-Y

1. INTRODUCTION

Bulk amorphous alloys (BAA) are of interest as potential next generation structural materials. Attractive mechanical and anti-corrosive properties of bulk amorphous alloys may be attributed to the unique atomic arrangements as well as defect free structures of BAAs [1,2]. The glass forming ability (GFA) of BAAs is very high, and hence fully amorphous materials can be prepared directly from liquids through advanced solidification processes [3].

In general, the composition ranges for BAAs are very narrow in multi-component alloy systems since the GFA of BAAs can be drastically decreased even with a slight compositional change of the alloy. Theoretical approaches to predict the composition range for BAAs have not yet been successful in practice. Consequently, empirical rules based upon the atomic size and heat of mixing between alloying elements have been widely used in alloy design for high GFA. The basic concept of the empirical rules is to stabilize liquid phase at low temperatures using more than three different alloying elements having large differences in atomic radii and large negative heats of mixing between them [4]. Since the atomic mobility is significantly decreased as temperature decreases, the liquid phase that is stabilized at low temperatures is readily frozen to an amorphous phase upon further cooling. Therefore, for the development of a new BAA, information on the phase equilibria is very important. Thus, finding a low melting composition range may be critical to the development of a new BAA.

*Corresponding author: yish@knu.ac.kr

In a Ni-Zr-Al system in which the empirical rules are satisfied, some Zr-rich composition ranges with high GFA have been reported, and thus Zr-based BAAs could be developed by adding fourth (or fifth) elements to Zr-rich ternary (or quaternary) alloys [5-7]. In light of cost and difficulty in materials processing, however, Ni-based BAAs in Ni-Zr-Al alloy systems are more attractive for extensive structural applications than Zr-based BAAs. Also, some properties of the Ni-based amorphous alloys, such as corrosion resistance, are expected to be superior to those of Zr-based amorphous alloys. In this study, Ni-based amorphous alloys with high GFA have been developed through systematic alloy design based upon the phase equilibria information of the Ni-rich corner and empirical rules for high GFA alloy design. The results of this study can serve as a foundation for the development of new Ni-based BAAs that have Ni, Al and Zr as main constituents.

2. ALLOY SELECTIONS

In the Ni-rich side of the Ni-Zr binary system, there exist two eutectic points, with Ni compositions of 91.2 % and 64 %, respectively [8]. A ternary intermetallic compound with the stoichiometry of $AlNi_2Zr$ has been reported [9]. The formation of a binary amorphous phase near the eutectic point of 64 % Ni has been reported while an amorphous phase formation near the eutectic point of 91.2 % Ni has not yet been reported [10]. Therefore, ternary alloy compositions between the binary eutectic point with 67 % Ni and a ternary intermetallic compound were selected for this study (Table 1).

Table 1. Nominal compositions and primary phase of Ni-Zr-Al ternary alloys

Alloy	Composition (at.%)			Primary phase
	Ni	Zr	Al	
#1	56	33	11	$AlNi_2Zr$
#2	53	32	15	$AlNi_2Zr$
#3	63	31	6	$Ni_{21}Zr_8$
#4	59	39	2	$Ni_{10}Zr_7$
#5	62	28	10	$AlNi_2Zr$
#6	57	28	15	$AlNi_2Zr$

3. EXPERIMENTAL PROCEDURE

Ingots of 15 g were prepared by a non-consumable arc-melting process under Ar atmosphere. In the arc-melting process, mixtures of high purity metallic elements (> 99.9 %) were melted more than four times to ensure chemical homogeneity. Rapidly quenched ribbons of 25-40 μm in thickness and 2-4 mm in width were prepared by a melt-spinning process. Pieces of a sliced ingot were inductively melted in a fused silica tube and quenched onto a copper wheel rotating at a wheel surface velocity of 30 m/sec. The phases present in specimens were identified by X-ray diffractometry (XRD) using Co-Kα and Cu-Kα. The as-cast microstructures were investigated by scanning electron microscopy (SEM) in backscattered image mode and the phase compositions were determined by the energy dispersive spectroscopy (EDS). The melting point of an alloy was determined by a differential thermal analyzer (DTA) using the as-cast sample in a fused alumina crucible. Glass transition and crystallization behaviors of amorphous ribbons were investigated by differential scanning calorimetry (DSC) with a heating rate of 0.67 K/sec.

4. RESULTS AND DISCUSSION

4.1. The as-cast microstructures

The as-cast microstructures and the XRD patterns of arc-melted samples are shown in Figs. 1 and 2, respectively. As listed in Table 1, the primary phases of as-cast microstructures can be classified into 3 different phases, $AlNi_2Zr$, $Ni_{21}Zr_8$, and $Ni_{10}Zr_7$. The ternary compound $AlNi_2Zr$ exists as a primary phase with dendrite morphology in the alloys containing more than 10 % Al (#1, #2, #5, and #6). As the alloy composition departs from the stoichiometric composition of $AlNi_2Zr$, the volume fraction of the primary $AlNi_2Zr$ phase decreases. Since the volume faction of the primary $AlNi_2Zr$ phase is very low in alloy #5, it is inferred that the alloy composition is located near the liquidus surface boundary of the $AlNi_2Zr$ phase. In the alloy $Ni_{63}Zr_{31}Al_6$ (#3), the $Ni_{21}Zr_8$ phase is the primary phase. This phase has lath morphology, and eutectic microstructure containing $Ni_{21}Zr_8$ and

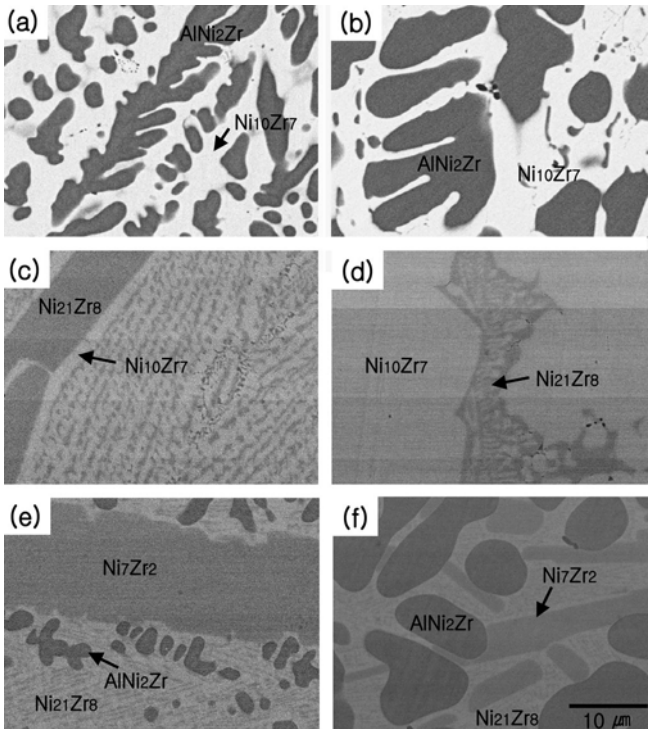

Fig. 1. Scanning electron micrographs (backscattered electron images) of as-cast Ni-Zr-Al ternary alloys: (a) alloy #1; (b) alloy #2; (c) alloy #3; (d) alloy #4; (e) alloy #5; and (f) alloy #6.

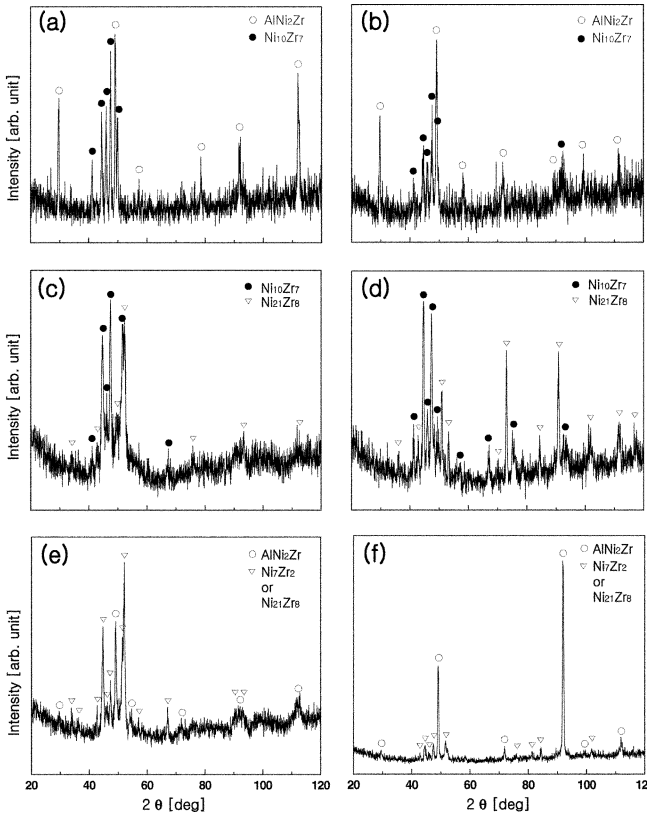

Fig. 2. XRD patterns of as-cast Ni-Zr-Al ternary alloys: (a) alloy #1; (b) alloy #2; (c) alloy #3; (d) alloy #4; (e) alloy #5; and (f) alloy #6.

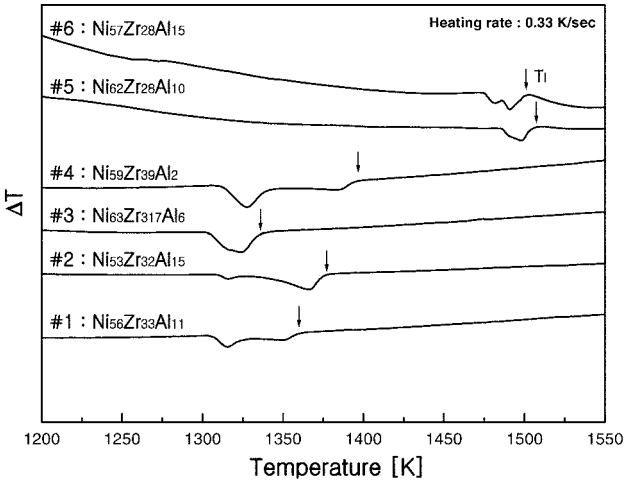

Fig. 3. DTA traces of as-cast Ni-Zr-Al ternary alloys.

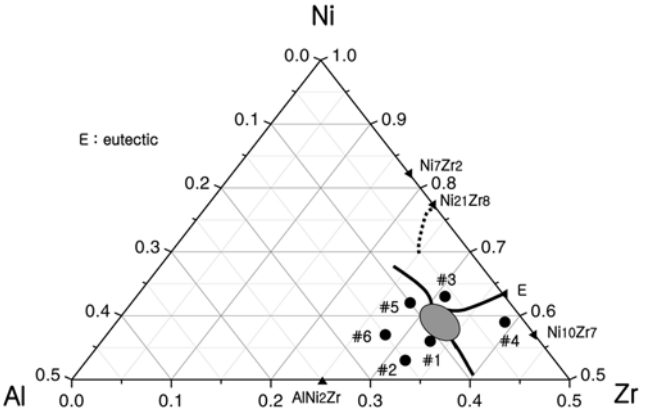

Fig. 4. Proposed partial liquidus projection in the Ni-rich corner of the Ni-Zr-Al ternary system.

$Ni_{10}Zr_7$ can be observed between the lath-type primary phases. In alloy #4, eutectic microstructure can also be observed between the primary phases of $Ni_{10}Zr_7$. Therefore, it can be inferred that the eutectic liquidus projection is extended from the Ni-Zr binary eutecitc point to the ternary region between the compositions of alloys #3 and #4. Based upon the DTA experimental results, the slope of the eutectic liquidus projection is thought to be slightly downward to the ternary region since the onset temperature of melting for alloy #3 is slightly lower than that for alloy #4 (Fig. 3). The temperature interval of melting for alloy #3 is quite narrow, indicating the alloy composition is near to the eutectic liquidus projection. Based on the results of the analysis of the as-cast samples, it can be inferred that the alloys in the composition range near the alloy $Ni_{63}Zr_{31}Al_6$ (#3) (the hatched area in Fig. 4) may exhibit relatively high glass forming ability (GFA), which is attributed to the low liquidus temperature.

4.2. Amorphous phase formation

The reduced glass transition temperature (T_{rg}) defined as the ratio of glass transition temperature (T_g) to liquidus temperature (T_l) has been conventionally used to assess the GFA of an alloy. As the T_{rg} increases, i.e., as the liquidus temperature decreases, the GFA of the alloy tends to increase. Based upon an analysis of conventional homogeneous nucleation theory, it is suggested that crystallization can be suppressed for T_{rg} higher than about 0.62 [11]. However, in reality, the critical T_{rg} values for amorphous phase formation vary as the alloy system changes. As an alternative parameter, the undercooled liquid region (ΔT_x), which can be defined as the temperature interval between the glass transition temperature and the crystallization temperature (T_x) upon heating the amorphous sample, has been recently used by Japanese research groups [12]. As the extent of ΔT_x of an amorphous alloy increases, stability of the liquid structure against crystallization tends to increase. Since the stability of the liquid structure of an alloy is closely related to the GFA of the alloy, most BAAs exhibit ΔT_x larger than 30 K [13]. Fig. 5 shows the DSC traces of the ternary alloy ribbons. The DSC trace of the alloy $Ni_{63}Zr_{31}Al_6$ (#3) having the lowest liquidus temperature among the ternary alloys clearly exhibits large DT_x indicating that the GFA of the alloy $Ni_{63}Zr_{31}Al_6$ (#3) has relatively high GFA among the ternary alloys. Since the alloy $Ni_{63}Zr_{31}Al_6$ (#3) seems to have slightly higher Ni content than that of the eutectic liquidus projection, a ternary alloy of $Ni_{60}Zr_{32}Al_8$ having the composition within the hatched area in Fig. 4 was selected for the high GFA multicomponent alloy design. To enhance GFA, several fourth elements that satisfy the empirical rules were added in the ternary alloy $Ni_{60}Zr_{32}Al_8$. In this study, we report the effects of Y addition on the GFA of the alloy $Ni_{60}Zr_{32-x}Al_8Y_x$. Since the atomic size of Y is very large and the Ni-Y mixing enthalpy is a large negative value, partial replacement of Zr with Y may enhance the GFA. Formation of a fully amorphous phase in the melt-spun ribbons of the alloys $Ni_{60}Zr_{32-x}Al_8Y_x$ can be

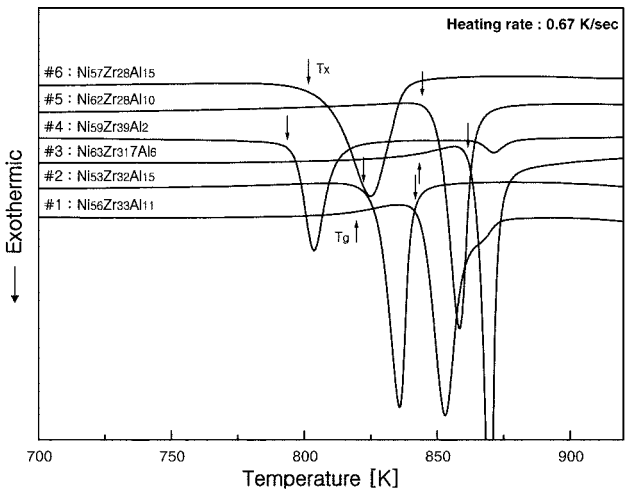

Fig. 5. DSC traces of the melt-spun ribbons of Ni-Zr-Al ternary alloys.

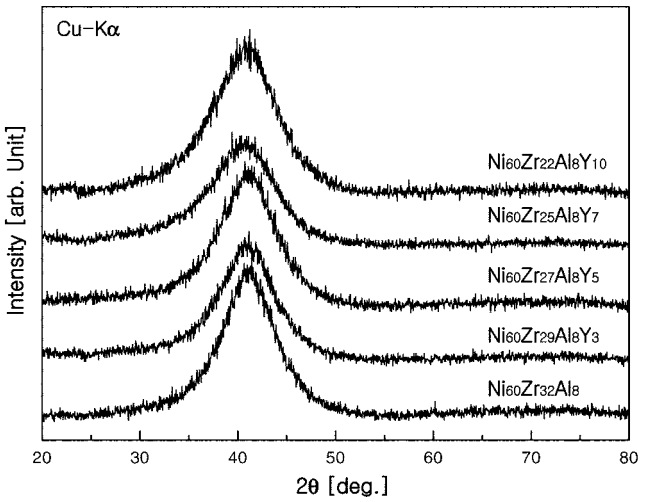

Fig. 6. XRD patterns of the melt-spun ribbons of $Ni_{60}Zr_{32-x}Al_8Y_x$ alloys (x=0, 3, 5, 7, 10).

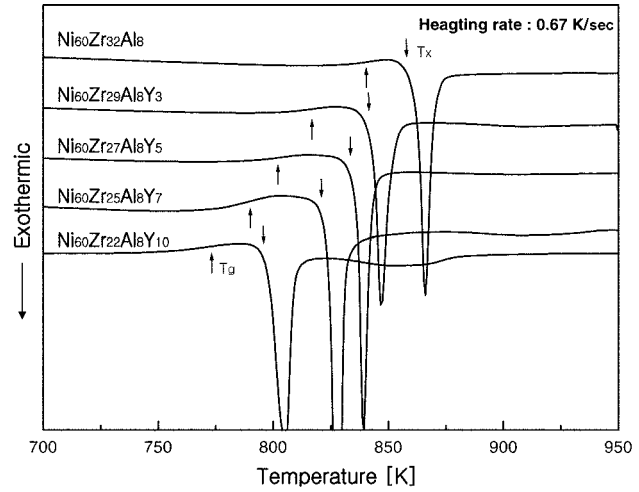

Fig. 7. DSC traces of the melt-spun ribbons of $Ni_{60}Zr_{32-x}Al_8Y_x$ alloys (x=0, 3, 5, 7, 10).

confirmed from the XRD results. Typical halo patterns for the amorphous phase were obtained and a diffraction peak could not be resolved, as shown in Fig. 6. The DSC traces of the ribbons shown in Fig. 7 indicate that an optimum amount of Y addition significantly increases the ΔT_x, i.e., the GFA of the $Ni_{60}Zr_{32-x}Al_8Y_x$ quaternary alloy. However, T_g and T_x of the $Ni_{60}Zr_{32-x}Al_8Y_x$ quaternary alloys monotonically decrease with an increase of Y content. The liquidus temperature significantly decreases with 3 % Y addition while only a slight increase of the liquidus temperature was observed with further addition of Y. Therefore, the T_{rg} values of the $Ni_{60}Zr_{32-x}Al_8Y_x$ quaternary alloys increases with a small amount of Y addition and then remains around 0.61 with further Y addition (Table 2). An alloy composition of $Ni_{60}Zr_{25}Al_8Y_7$ with high T_{rg} and ΔT_x was prepared in rod form by an injection casting method. As can be inferred from the DSC trace shown in

Table 2. Nominal compositions and thermal properties of quaternary $Ni_{60}Zr_{32-x}Al_8Y_x$ alloys (x=0, 3, 5, 7, 10)

Alloy	T_g [K]	T_x [K]	ΔT_x [K]	T_l [K]	T_{rg}
$Ni_{60}Zr_{32}Al_8$	841	862	21	1439	0.59
$Ni_{60}Zr_{29}Al_8Y_3$	818	844	26	1331	0.61
$Ni_{60}Zr_{27}Al_8Y_5$	803	836	33	1312	0.61
$Ni_{60}Zr_{25}Al_8Y_7$	790	825	35	1298	0.61
$Ni_{60}Zr_{22}Al_8Y_{10}$	771	797	26	1263	0.61

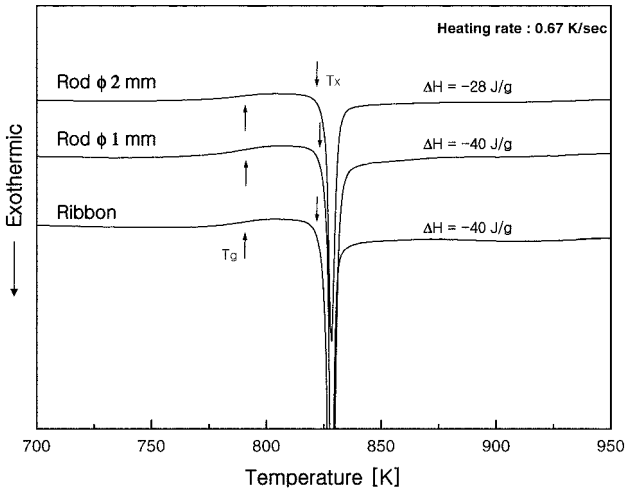

Fig. 8. DSC traces of the injection cast rods and ribbon of $Ni_{60}Zr_{25}Al_8Y_7$.

Fig. 8, the amorphous phase was formed in rods of 1 mm and 2 mm in diameter, respectively. Since the amount of heat released during crystallization of the rod with the diameter of 1 mm is the same as that of the ribbon (40 J/g), the rod can be considered fully amorphous. Most Ni-based bulk amorphous alloys developed to date contain non-metallic elements such as P or Si [14]. Therefore, the Ni-based bulk amorphous alloy developed in the alloy system Ni-Zr-Al-Y comprising only metallic elements may have unique properties that can potentially expand practical applications of the bulk amorphous alloys.

5. CONCLUSIONS

Ni-based bulk amorphous alloys comprising only metallic elements have been developed in the alloy system Ni-Zr-Al-Y system. For an alloy design for high GFA, finding composition ranges with low liquidus temperatures is important since the GFA of the alloy is closely related to the liquidus temperature. As an additional element to enhance GFA of the ternary $Ni_{60}Zr_{32}Al_8$ alloy, small additions of yttrium satisfying empirical rules for high GFA alloy design was very effective. With the optimum replacement of Zr with Y, the GFA of the quaternary alloys could be significantly increased. To demonstrate high GFA of the alloy $Ni_{60}Zr_{25}Al_8Y_7$, a fully amorphous rod 1 mm in diameter was prepared through an

injection casting method. The amorphous rod exhibited high T_{rg} (0.61), ΔT_x (35K) and ΔH (40 J/g), corresponding to those of the ribbon of the alloy.

ACKNOWLEDGMENTS

This work was financially supported by MOCIE (Ministry of Commerce, Industry and Energy) under the development of structural metallic materials and parts with super strength and high performance project.

REFERENCES

1. R. Busch, A. Masuhr, and W. L. Johnson*, Mater. Sci. Eng. A* **304-306**, 97 (2000).
2. A. Inoue and T. Zhang, *Mater. Trans. JIM* **37**, 1726 (1996).
3. A. Inoue, *Bulk Amorphous Alloys Preparation and Fundamental Characteristics*, p. 27, Trans Tech Publication Ltd., Switzerland (1998).
4. A. Inoue, *Mater. Trans. JIM* **36**, 866 (1995).
5. W. Chen, Y. Wang, J. Qiang, and C. Dong, *Acta metall. mater.* **51**, 1899 (2003).
6. Z. J. Yan, F. Li, S. R. He, and Y. H. Zhou, *Mater. Lett.* **57**, 1840 (2003).
7. L. Q. Xing, P. Ochin, F. Faudot, M. Harmelin, J. Bigot, and J. P. Chevalier, *Mater. Sci. Eng. A* **220**, 155 (1996).
8. T. B. Massalski, *Binary Alloy Phase Diagrams*, 2nd edition, p. 2889, ASM Int., Materials Park, Ohio (1990).
9. P. Villars, A. Prince, and H. Okmoto, *Handbook of Ternary Alloy Phase Diagrams*, p. 4240, ASM Int., Materials Park, Ohio (1995).
10. Y. A. Babanov, V. R. Schvetsov, and A. F. Sidorenko, *Phys. B* **208-209**, 375 (1995).
11. J. F. Löffler, *Intermetallics* **11**, 529 (2003).
12. A. Inoue, *J. Non-Cryst. Solids* **156-158**, 473 (1993).
13. A. Inoue, *Acta mater.* **48**, 279 (2000).
14. S. Yi, J. K. Lee, W. T. Kim, and D. H. Kim, *J. Non-Cryst. Solids* **291**, 132 (2001).